Molecular Cell *24*, 383–395, November 3, 2006 ©2006 Elsevier Inc. DOI 10.1016/j.molcel.2006.09.006

Molecular Basis of AKAP Specificity for PKA Regulatory Subunits

Matthew G. Gold,[1,4] Birgitte Lygren,[2,3,4] Pawel Dokurno,[1] Naoto Hoshi,[3] George McConnachie,[3] Kjetil Taskén,[2] Cathrine R. Carlson,[2,3] John D. Scott,[3] and David Barford[1,*]

[1] Section of Structural Biology
Institute of Cancer Research
Chester Beatty Laboratories
237 Fulham Road
London SW3 6JB
United Kingdom

[2] Biotechnology Centre
University of Oslo
P.O. Box 1125
Blindern, N-0317 Oslo
Norway

[3] Howard Hughes Medical Institute
Vollum Institute
Oregon Health and Science University
Portland, Oregon 97239

Summary

Localization of cyclic AMP (cAMP)-dependent protein kinase (PKA) by A kinase-anchoring proteins (AKAPs) restricts the action of this broad specificity kinase. The high-resolution crystal structures of the docking and dimerization (D/D) domain of the RIIα regulatory subunit of PKA both in the apo state and in complex with the high-affinity anchoring peptide AKAP-*IS* explain the molecular basis for AKAP-regulatory subunit recognition. AKAP-*IS* folds into an amphipathic α helix that engages an essentially preformed shallow groove on the surface of the RII dimer D/D domains. Conserved AKAP aliphatic residues dominate interactions to RII at the predominantly hydrophobic interface, whereas polar residues are important in conferring R subunit isoform specificity. Using a peptide screening approach, we have developed SuperAKAP-*IS*, a peptide that is 10,000-fold more selective for the RII isoform relative to RI and can be used to assess the impact of PKA isoform-selective anchoring on cAMP-responsive events inside cells.

Introduction

cAMP-dependent protein kinase (PKA) has served as a paradigm in several biological contexts. It first came to prominence 50 years ago as the predominant intracellular receptor for cAMP, acting downstream of G protein-coupled receptors via the activation of adenylyl cyclase. The resulting PKA phosphorylation events exert diverse biological effects by changing the activity of a range of protein substrates (Shabb, 2001). The broad-substrate specificity of PKA is directed toward specific intracellular substrates by a multigene family of AKAPs. AKAPs serve to target PKA to distinct subcellular loci and coordinate multiple signaling enzymes in supramolecular complexes. This scaffolding function permits optimal spatiotemporal resolution and integration of signal transduction pathways (Wong and Scott, 2004). Characterization of these complexes is critical to understand signaling pathway integration (Pawson and Scott, 1997; Smith et al., 2006).

The PKA holoenzyme is a tetramer of two catalytic subunits (C) that are maintained in an inactive conformation by a regulatory (R) subunit dimer. R subunit association with cAMP releases the active C subunits to permit phosphorylation in the local vicinity (reviewed in Wong and Scott [2004]). Through its N-terminal D/D domain, the R subunit dimer of PKA associates with an amphipathic helix of 14–18 residues common to all AKAPs (Carr et al., 1991). Since the identification of the first AKAP (Lohmann et al., 1984; Vallee et al., 1981), over 50 members of the family are now known, with roles in the modulation of ion channels (Johnson et al., 1994; Rosenmund et al., 1994; Westphal et al., 1999), insulin secretion (Alto et al., 2002; Zhang et al., 2005), cardiac function (Fink et al., 2001), auditory fear (Moita et al., 2002), and lipoprotein lipase translation (Ranganathan et al., 2005). The potential for multivalency in AKAPs, first demonstrated for AKAP79 (Klauck et al., 1996), is now recognized as a common mechanism to mediate signal integration. Variations on this theme are exemplified by mAKAP (Dodge-Kafka et al., 2005) and AKAP-Lbc (Carnegie et al., 2004). Importantly, AKAPs are also responsible for differential targeting of the two R subunit isoforms, conferred by RI, RII, or dual-specificity AKAPs (Angelo and Rubin, 1998; Huang et al., 1997; Li et al., 2001). R type specificities of different AKAPs have also been characterized in vitro (Herberg et al., 2000), and the only disease-related SNP identified in an AKAP to date alters R subunit specificity (Kammerer et al., 2003).

The structural basis for the AKAP-D/D interaction has been studied by NMR for the RIIα D/D domain (Newlon et al., 2001) and more recently modeled by using an NMR structure of the RIα D/D domain (Banky et al., 2003). The general binding mode is established for RIIα, with the AKAP helix binding diagonally to a hydrophobic surface of a four-helix bundle formed by the two RII D/D domains. However, information regarding site-specific intermolecular amino acid contacts, crucial for defining R subunit specificity, remains to be established.

Several studies aimed at identifying the sequence determinants for AKAP binding have established the crucial role of hydrophobic residues on one face of the helix (Miki and Eddy, 1999). In RIIα, residues $Ile3^R$ and $Ile5^R$ (superscript "R" denotes residues of RIIα) have been proposed as key binding determinates (Hausken et al., 1996), and peptide substitution arrays have been used to derive high-affinity AKAP peptides (Alto et al., 2003; Burns-Hamuro et al., 2003). In a previous study, Alto and colleagues employed bioinformatic and peptide-array screening approaches to generate a reagent, AKAP-*IS*, which binds RIIα with a K_d of 0.4 nM, an affinity

*Correspondence: david.barford@icr.ac.uk
[4] These authors contributed equally to this work.

Table 1. Crystallographic Data Statistics

Collection and MAD Phasing Statistics					
		RII Apo (Leu9 → Met)			
Data Set	RII (1-43) Apo Wild-Type	Inflection	Peak	Remote	RII (1-45)-AKAP-*IS*
X-ray source	SRS PX14.2	SRS PX9.5			ID29 ESRF
Space group	$P6_522$	$P6_522$			$P2_12_12_1$
Unit cell (Å)	a = b = 91.5	a = b = 92.6			a = 41.352, b = 45.251
	c = 189.0	c = 189.3			c = 56.837
Z	8	8			1
Wavelength (Å)	1.488	0.9792	0.9778	0.935	0.970
Resolution (Å)	2.20	2.50	2.50	2.60	1.30
Observations (N)	655,976	282,662	371,582	280,040	116,862
Unique reflections (N)	23,415	17,274	17,297	15,435	26,863
Completeness (%)	100.0 (88.2)	95.7 (97.1)	99.9 (100)	99.3 (98.5)	99.7 (99.8)
Anomalous completeness (%)	-	95.1	99.7	96.9	–
R_{merge}	0.072 (0.244)	0.076 (0.23)	0.065 (0.18)	0.061 (0.21)	0.058 (0.341)
R_{anom}	–	0.065 (0.22)	0.065 (0.18)	0.061 (0.21)	–
$I/\sigma(I)$	11.6	10.4	13.0	12.5	16.0
Phasing power acentric/centric	–	0.78/0.53	0/0	1.21/0.77	–
Anomalous phasing power	–	1.66	3.23	2.38	–
R_{Cullis} acentric/centric	–	0.79/0.82	0/0	0.82/0.82	–
Anomalous R_{Cullis}	–	0.84	0.57	0.76	–
Refinement					
Resolution range (Å)	30.0–2.20				35.40–1.30
Reflections (N)	21,445 (100%)				25,468 (100%)
Number of nonhydrogen atoms (N)	3280				915
R value	0.215				0.164
Free R value (N reflections)	0.271 (1,970)				0.194 (1,273)
Deviation from ideality					
Bond angles (Å)	0.011				0.018
Bond lengths (°)	1.253				1.805
Average B factor ($Å^2$)	22.1				15.243
Ramachandran values (preferred/allowed/disallowed)	96.4%/3.7%/0.0%				96.2%/3.8%/0.0%

some 5-fold higher than for the AKAP-Lbc derived peptide Ht31 (Alto et al., 2003).

Here, we describe the crystal structure of the D/D domain of RIIα in complex with an AKAP (AKAP-*IS*), providing a molecular explanation of AKAP and RIIα-subunit sequence recognition determinants and a framework for rationalizing the results of peptide-array screening data. Although AKAP-*IS* binds well to RIIα and has some affinity for RIα, we have now explored specificity of the R subunit-AKAP interaction and have developed an improved reagent, SuperAKAP-*IS*, through a peptide screening approach. SuperAKAP-*IS* has some 4-fold higher affinity for RIIα and 12.5-fold reduced affinity for RIα compared to AKAP-*IS,* as judged by peptide screening. The peptide-array screening data and crystal structure provide insight at the molecular level into the determinants of high-affinity binding to RII and for R subunit selectivity.

Results

The Apo RIIα D/D Dimer Forms an X Type Four α Helix Bundle

We first determined the crystal structure of the apo RIIα D/D dimer (residues $Ser1^R$–$Arg43^R$ [symmetry-related protomer is denoted "R prime"]) to 2.2 Å resolution (Table 1). Two RIIα D/D domains dimerize to form an X type four-helix bundle, with an antiparallel arrangement of the two RIIα D/D domain α helices (denoted A and B) (Figure 1A). Four independent RIIα D/D dimers generated from eight individual protomers comprise the crystal asymmetric unit. As judged from pair-wise structural comparisons, the protomers adopt essentially identical conformations, with an average root-mean-square deviation (rmsd) between equivalent Cα atoms of 0.2 Å, with only small differences in the conformation of solvent-exposed Arg side chains (Table S1 in the Supplemental Data available with this article online) (Figure 1C). For all molecules, the two N-terminal residues ($Ser1^R$ and $His2^R$) are disordered. Electron density corresponding to the main chain of $Ile3^R$ is visible in five molecules, although its side chain is ordered in only three of these. For three other protomers, the polypeptide chain become structured at $Gln4^R$ (Figure 1C and Table S1). The N-terminal three residues of RIIα D/D therefore represent a relatively mobile region of the RIIα D/D subunit, with the conformation of $Ile3^R$ restrained by AKAP interactions (see below).

AKAP-*IS* Engages a Shallow Hydrophobic Groove on RII D/D

We determined the AKAP-*IS*-RIIα D/D complex to 1.3 Å resolution (Table 1) (Figure 1B). The 18 residues of AKAP-*IS* (Gln4–Lys21) (Figure 2A) are well resolved in electron density, except for the side chain of Gln4. AKAP-*IS* forms five turns of an amphipathic α helix, lying diagonally (~50°) across one face of the symmetrical RII dimer of the N-terminal helices (A and A′) of each RIIα subunit (Figure 1B). Due to crystal contacts, an asymmetric orientation of the RIIα-AKAP-*IS* complex is

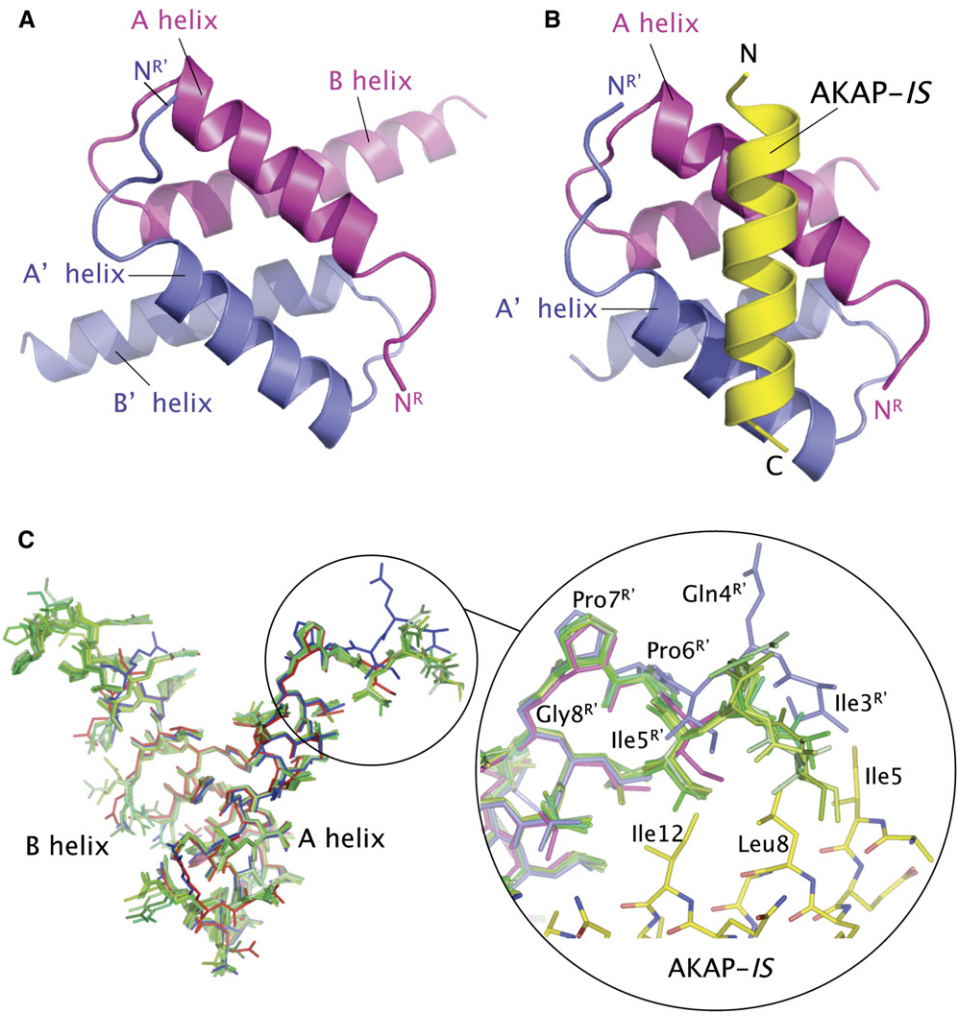

Figure 1. Overview of Structures of RII D/D and Its Complex with AKAP-*IS*

(A) Apo RII D/D structure showing formation of an X type four-helix bundle by two RIIα chains with protomers 1 and 2 colored magenta and blue, respectively, viewed along the dyad axis.

(B) RII D/D AKAP-*IS* complex with the AKAP-*IS* helix (colored yellow) binding at a surface of two RII D/D promoters formed by the two N-terminal helices (αA and αA′). Residues (5^{R}–43^{R}) and ($3^{R'}$–$43^{R'}$) are visible in the electron density for protomers 1 and 2, respectively. The N terminus of AKAP-*IS* is in close proximity to the N terminus of the first helix of promoter 2 (αA′) rather than protomer 1 (αA).

(C) Superpositions of the N termini of the eight RIIα D/D protomers from the apo crystal structure and two from the complex with AKAP-*IS*. Each protomer of apo RII D/D is colored a shade of green, with the promoters of the RII D/D-AKAP-*IS* complex colored magenta and blue as in (A) and (B). The position of AKAP-*IS* relative to αA′ is illustrated in close up, to show the conformational difference of $Ile3^{R'}$–$Ile5^{R'}$ of protomer 2 (blue) of the complex relative to apo D/D and protomer 1 of the RII-AKAP-*IS* complex.

generated whereby AKAP-*IS* adopts a unique polarity across the RII-subunit AKAP interface. Interestingly, the symmetry of the AKAP-interaction interface within the RII D/D homodimer is reflected in a pseudo 2-fold symmetry of the AKAP-*IS* primary structure centered on residues Asp14 and Asn15 (Figures 2A and 2B). These two residues define the position within AKAP-*IS* that bisects the RII D/D dyad axis within the RII-AKAP-*IS* complex (Figure 2B). A symmetrical pattern of hydrophobic and hydrophilic amino acids is centered on these two residues, illustrating how an asymmetric α helix interacts with a symmetrical interface. However, notable asymmetry is introduced into the RIIα-AKAP-*IS* complex by the ordering of two additional residues ($Ile3^{R'}$ and $Gln4^{R'}$) at the N terminus of αA′ relative to αA of RII, promoted by its interactions with Ile5 and Leu8 of AKAP-*IS* (Figures 1C, 2C, and 4). In the opposite protomer, $Ile5^{R}$ is the first ordered N-terminal residue. Overall, the two RII D/D protomers of the RII-AKAP-*IS* complex are very similar; equivalent Cα atoms superimpose within 0.5 Å, essentially identical to their individual differences with the apo RII D/D structure (Table S1 and Figure 1C). Moreover, the relative orientations of RII D/D protomers within the dimer are similar in the apo and complex structure (rmsd between equivalent Cα atoms of 0.6 Å), suggesting that, apart from the N-terminal two residues of one RII D/D protomer, the tertiary and quaternary conformations of RII D/D do not change on association with AKAP-*IS*.

A prominent AKAP binding channel on RIIα measuring 8 by 30 Å accommodates the amphipathic AKAP-*IS* α helix (Figures 3A and 3D). Residues Ile5–Lys21 of AKAP-*IS* interact with RIIα (defined at interatom distances <4 Å). Notably, two AKAP-*IS* residues, Ile5 and Ala20, define the critical N- and C-terminal anchor points

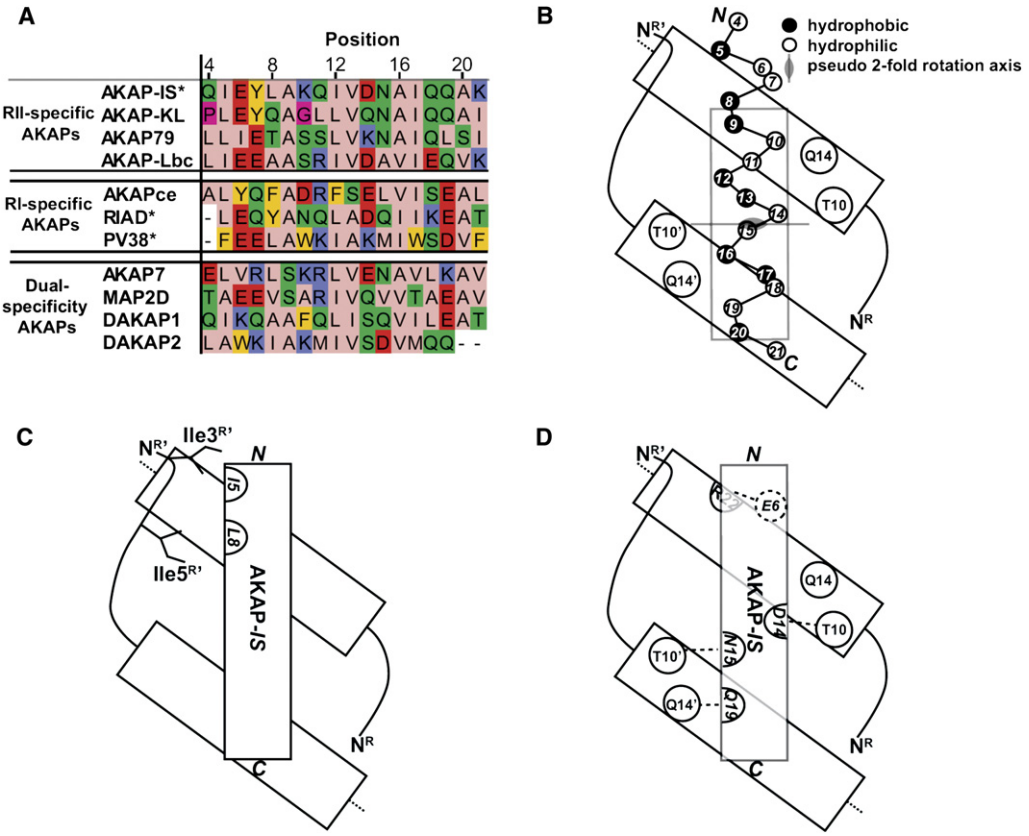

Figure 2. Analysis of AKAP-Specific R Subunit Interactions

(A) Alignment of the R subunit binding regions of AKAPs in three classes is shown with residues numbered according to SuperAKAP-*IS*. Artificially designed AKAP sequences are marked with asterisks.

(B) Pseudo-2-fold symmetry of AKAP-*IS* provides a helix for binding to a symmetrical interface: the periodicity of hydrophilic and hydrophobic residues around the pseudo-2-fold symmetry axis in AKAP is illustrated.

(C) The flexible region of Ile3$^{R'}$–Ile5$^{R'}$ in close proximity to the N terminus of AKAP-*IS* is illustrated.

(D) H bonding hot spots: the positions of residues in AKAP-*IS* that contact RIIα outside of the hydrophobic core are illustrated. Three contacts are to the [Gln10^{R}–Thr14^{R}] pairs in RIIα.

of the peptide at the RIIα-AKAP-*IS* interface (Figures 3A and 3C).

Nonpolar and Polar Interactions Contribute to High-Affinity AKAP-*IS* Binding

Core Hydrophobic Interactions

As expected, hydrophobic interactions between AKAP-*IS* and the RIIα D/D dominate the 1433 Å^2 solvent-accessible surface area buried at the RII D/D-AKAP-*IS* interface. Four short-chain nonpolar aliphatic residues of AKAP-*IS* (Ala9, Val13, Ala16, and Ala20) project toward the center of the hydrophobic face presented by RIIα and are completely buried at the interface. In contrast, longer aliphatic residues (Ile5, Leu8, Ile12, and Ile17*)* project from the sides of the helix and are partially solvent exposed (Figure 3). Together, these residues create a hydrophobic ridge running along the AKAP helix axis, forming intimate associations with the predominantly hydrophobic surface of the RII AKAP interface (Figure 3A). The nonpolar-AKAP interface of RIIα is formed from the side chains of tightly interpacked aliphatic residues; bulky aromatic residues do not participate (Figure 3B). Thus, a rigid, relatively featureless shallow surface is created, lacking distinct cavities or protrusions, complementary to the uniform hydrophobic surface of AKAP-*IS* (Figures 3B and 3D). Water molecules are excluded from the RII-AKAP interface, whereas Thr17^{R} and Thr17$^{R'}$ in RIIα are the only polar-buried residues. The interactions between residues Ile5 and Leu8 of AKAP-*IS* and Ile3$^{R'}$ and Ile5$^{R'}$ in αA$'$ are notable (Figures 2C and 4A): Ile3$^{R'}$ and Ile5$^{R'}$ had previously been proposed as essential components of the RIIα interface, and the absence of Pro7$^{R'}$ in RIIβ was suggested as a means to distinguish between the two RII isoforms (Hausken et al., 1994), potentially accounting for the 4-fold weaker affinity for the β isoform displayed by D-AKAP2 (Burns et al., 2003). Hydrogen/deuterium exchange data, which showed free exchange of these isoleucines in complex with AKAP peptides (Fayos et al., 2003), apparently in conflict with our structure, are in fact due to the asymmetric binding of AKAP to the RII interface, leaving one N terminus of RII solvent-exposed (Figures 2D and 4).

Other Sequence-Dependent RII-AKAP Interactions

A striking feature of the structure is that the RII residue pairs [Thr10^{R}; Gln14^{R}] and [Thr10$^{R'}$; Gln14$^{R'}$], on opposite corners of the D/D interface, are well positioned to interact with exposed AKAP-*IS* side chains. Asp14 of AKAP-*IS* accepts a hydrogen bond from Thr10^{R} (Figures

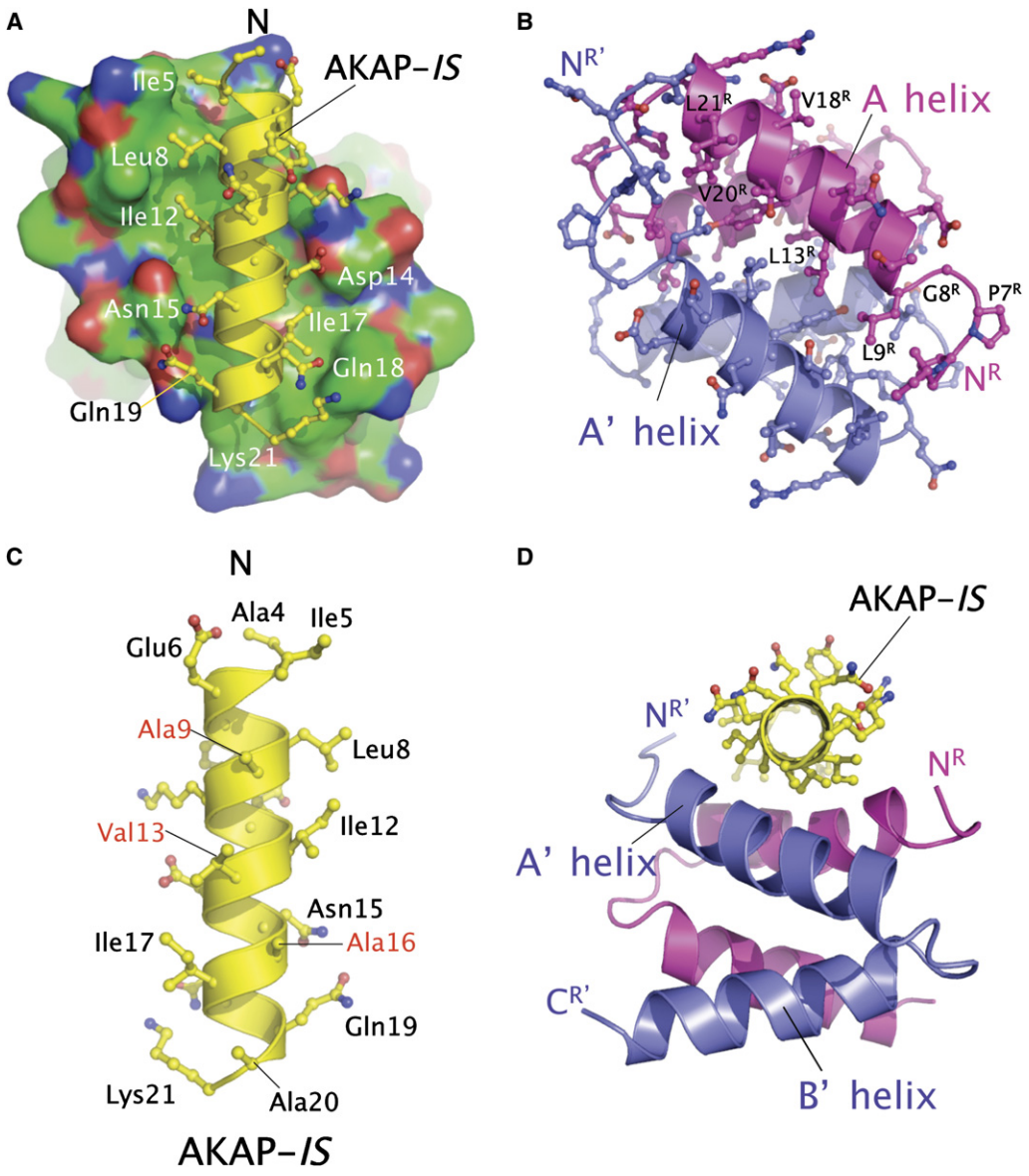

Figure 3. Core Hydrophobic Interface

(A) Surface representation of the RIIα D/D dimer with AKAP-*IS* helix shown as ribbons and ball and stick engaged within the AKAP binding groove, view as in Figure 1B.

(B) RII D/D dimer orientation as in (A) showing the antiparallel orientation of the A helices. Aliphatic residues at the AKAP-*IS* interface are labeled in protomer 1.

(C) View of the hydrophobic ridge of AKAP-*IS* that interacts with RII. Red-labeled residues are totally buried at the interface.

(D) Ribbon representation of RII D/D and AKAP-*IS* with side chains of AKAP-*IS* indicated.

2D and 4B), and Gln19 of AKAP-*IS* is H bonded to Gln14$^{R'}$ (Figures 2D and 4A). The side chain of Thr10$^{R'}$, which lacks the potential to H bond with Asp14 of AKAP-*IS*, instead forms a water-mediated contact to Asn15 (Figures 2D and 4A).

Helix-Stabilizing Interactions within AKAP-IS

Helix-stabilizing interactions within the AKAP helix had previously been suggested as a mechanism to increase affinity (Alto et al., 2003). In our structure, we note three interactions within AKAP-*IS* that are likely to stabilize the helix. Between adjacent turns there is a stacking interaction between Tyr7 and Gln11 and an H bond between Asn15 and Gln19 (Figure 4A). Gln19 therefore participates in a network of H bonds involving Asn15 and, as noted above, Thr10$^{R'}$ and Gln14$^{R'}$ of RII (Figure 4A). Significantly, RII-peptide array analysis revealed that an Asn is preferred at position 15 in the AKAP helix (Alto et al., 2003), and Asn and Gln at positions 15 and 19, respectively, are conserved within RII-specific AKAPs (Figure 2A). In addition, the side chain of Glu6 folds back to satisfy an H bond to its backbone amino group in a classical helix-capping interaction (Figure 4B). Interestingly, previous reports had predicted that Glu6 would form an intrahelix salt bridge with Lys10, accounting for its ability to stabilize AKAP-RII interactions (Alto et al., 2003), whereas we find that the two charged side chains

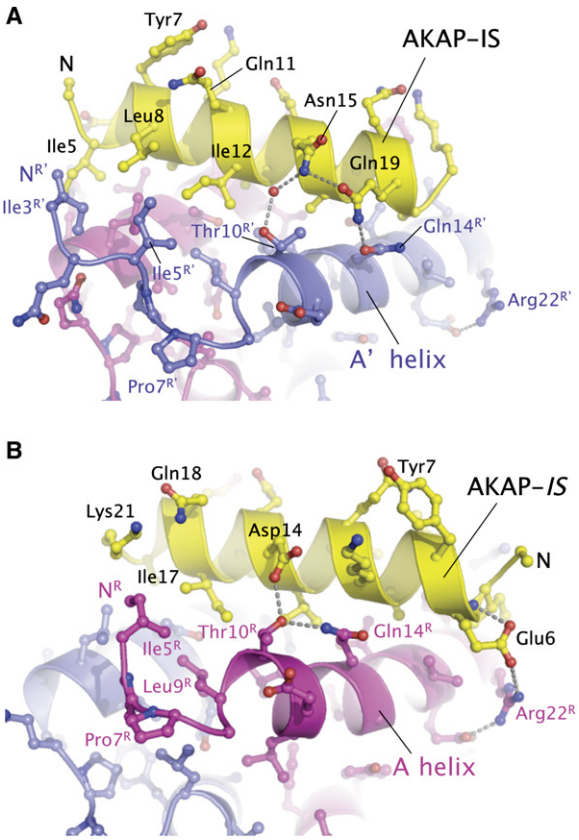

Figure 4. Details of the AKAP-*IS*-RIIα D/D Polar Contacts

(A and B) Two detailed views of the interface between AKAP-*IS* (colored yellow) and αA′ (blue) and αA (magenta) of RII D/D.

are positioned some 10 Å apart. The side chain of Glu6 also forms a long salt bridge with the guanidinium side chain of Arg22^{R} (Figure 4B). In the RIIα-AKAP-*IS* complex, Lys10 is exposed to solvent, and the ability of a lysine at this position to optimize interactions with RII is not readily apparent.

Comparison to Other R Subunit D/D Structures

Apo RIIα Crystal Structure

A comparison of the RII-AKAP-*IS* complex with the 2.2 Å resolution crystal structure of apo RIIα reveals that RII presents a predominantly rigid docking surface for the engagement of AKAPs. The two RII D/D structures are essentially identical, superimposing within an rmsd of 0.6 Å for equivalent Cα atoms (Table S1). Significantly, side chain conformations of residues forming the AKAP binding surface vary little between the two structures: the hydrophobic residues at positions 9, 13, 18, 20, and 21 superimpose with an rmsd of 0.6 Å for all atoms. The N-terminal region containing residues Ile3$^{R'}$–Ile5$^{R'}$ in protomer 2 represents the largest difference between the apo and complex conformations of RII D/D (Figures 1C and 4). In the RII-AKAP-*IS* structure, Ile3$^{R'}$ and Gln4$^{R'}$ of protomer 2 are well defined but disordered in protomer 1. Compared to their conformations in the apo structure, residues Ile3$^{R'}$–Ile5$^{R'}$ shift by 2–3 Å in the complex to avoid steric clashes with Ile5, Leu8, and Ile12 of AKAP-*IS* (Figures 1C and 4). The conformation of Ile5^{R} in protomer 1 in the RII-AKAP-*IS* complex is essentially unchanged relative to the apo structures (Figure 1C). Notably, the N-terminal residues of protomer 2 (Ile3$^{R'}$–Ile5$^{R'}$) that shift position on forming the complex contribute only 9% of the total buried area at the RII D/D-AKAP-*IS* interface. Outside of the core hydrophobic interface, alternative rotamer conformations are observed for the side chains of Thr10^{R}, Gln14$^{R'}$, and Arg22^{R}, all of which contact AKAP-*IS* (Figure 4).

NMR RIIα-Ht31 Structure

The NMR structure of RIIα-Ht31 differs from our structure in a number of respects. The RII D/D dimers superimpose with an rmsd of 1.4 Å for equivalent Cα-atoms, with the largest differences occurring at the two N termini (Figure 5A). In the NMR structure, the AKAP peptide Ht31 binds ~25° more parallel to the N-terminal RII helices than AKAP-*IS*. The two AKAP peptides are very similar (Figure 2A, Ht31 represents the RII binding sequence in the multifunctional anchoring protein AKAP-Lbc) and would be expected to share the same binding mode. In the NMR structure, the critical Ile3^{R} residues at the two N termini of the RII dimer face away from Ht31 into solution. As previously noted by the authors, this is likely to be an artifact arising from the presence of a partial His tag at each N terminus that is expected to be protonated at the low pH (pH 4) of the NMR experiment (Newlon et al., 2001). Furthermore, accurately positioning the AKAP helix by NMR is challenging due to the 2-fold symmetry of the RII interface.

RIα D/D Apo NMR Structure

Core residues in the two D/D subunits (residues 9^{R}–43^{R} in RIIα) align with an rmsd of 1.8 Å for equivalent Cα atoms, unusually high considering the 29% sequence identity between the two human R subunits (Figure 5B). The isoform-specific docking region of RIα (Banky et al., 2003) is similarly positioned to the Ile3$^{R'}$/Ile5$^{R'}$ region of RIIα, and the binding mode of AKAP to the D/D surface is likely to be similar for the two R subunit isoforms.

RIIα D/D-D-AKAP2 Crystal Structure

In parallel work to ours, Taylor and colleagues (Kinderman et al., 2006 [this issue of *Molecular Cell*]) have determined the crystal structure of RIIα D/D in complex with a peptide corresponding to D-AKAP2. The RII D/D dimers superimpose closely (rmsd 0.65 Å for Cα atoms, with conserved side-chain conformations). The two AKAPs engage RII in the same register but are rotated by a small angle of 6°, such that 17 equivalent Cα atoms superimpose with an rmsd of 1.5 Å.

Optimization of AKAP-*IS* to Yield an RIIα-Specific Peptide

In order to learn more about the specificity of R subunit-AKAP interactions, we used AKAP-*IS* that binds both RII and RI with low and high nanomolar affinity, respectively (Alto et al., 2003), as a starting point for further rounds of two-dimensional peptide array screening to find specific determinants for AKAP interaction with RIIα and RIα. The goal of these studies was to develop an RII-specific anchoring disruptor. Analysis of 340 AKAP-*IS* peptide derivatives where each residue in AKAP-*IS* (given by its single-letter code above each array) was replaced by all 20 amino acids (given by their single-letter codes to the left of each array) was conducted by overlay assays (Figure 6). R binding was analyzed by RIIα-^{32}P (Figure 6A)

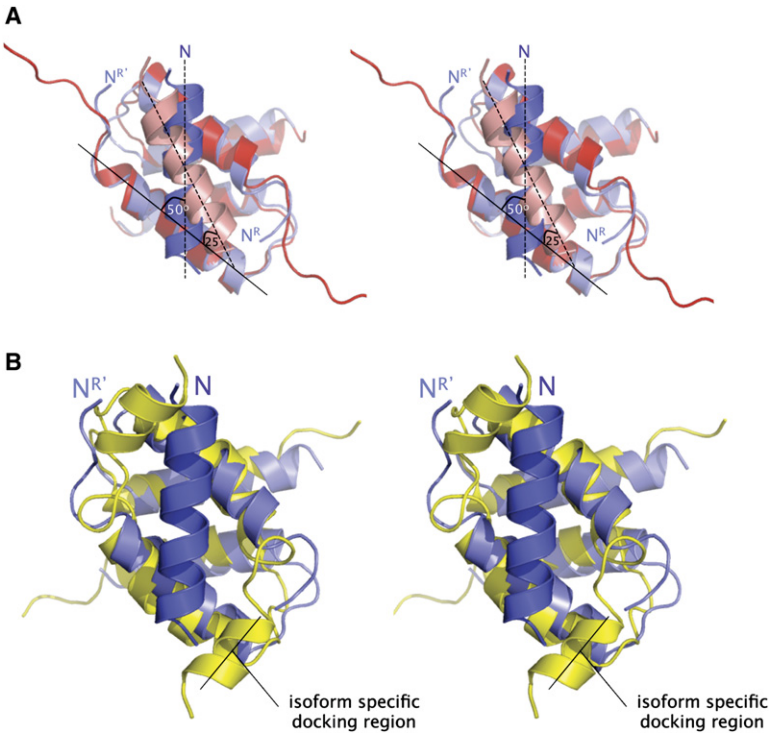

Figure 5. Comparison to Other R Subunit D/D Structures

Stereoviews. (A) Crystal structure of the RII D/D-AKAP-*IS* complex (RII D/D protomers in light blue, AKAP-*IS* in dark blue) superimposed onto the NMR RIIα D/D-Ht31 complex structure (RII D/D protomers red, Ht31 in salmon) and (B) RIIα D/D of our RII D/D-AKAP-*IS* (blue) with the apo RIα D/D NMR structure (yellow).

or RIα-^{32}P overlay (Figure 6B) and detected by autoradiography. The apparent binding affinity of each modified peptide was compared with the signal strength of internal control peptides (AKAP-*IS*) in the upper row and distributed throughout the array (white circles). The preferred positions of the substitutions were 8, 11, 15, 16, 18, 19, and 20 (marked with red circles). Interestingly, L8H, L8K, or L8V substitution decreased RIα binding dramatically, whereas apparent RIIα affinity was increased. Fifteen peptides with lower affinity for RIα and higher affinity for RIIα (out of 40 modified peptide derivatives with single, double, and triple substitutions tested) are shown in Figure 6C. The relative RIIα and RIα binding was measured by densitometry analysis of the autoradiographs (n = 3). In the filter assays, the peptide with the triple substitutions L8V, N15Y, and Q18H (denoted with a star in Figure 6C) had a four times higher apparent affinity for RIIα compared to that of AKAP-*IS*. This peptide, named SuperAKAP-*IS* (QIEYVAKQIVD YAIHQA), exhibited the most RII-selective profile. The SuperAKAP-*IS* peptide exhibited a 12.5 times lower apparent affinity for RIα but retained its high affinity for RII.

SuperAKAP-*IS* Is Selective for RII

SuperAKAP-*IS* was cloned with preferred codon usage and fused to the C terminus of GFP. Lysates from HEK293 cells transfected with GFP, GFP-AKAP-*IS*, GFP-SuperAKAP-*IS*, and GFP-scrambledAKAP-*IS* were separated by PAGE and R binding analyzed by RIα-^{32}P and RIIα-^{32}P overlay (Figure 7A, middle and top panels, respectively). Whereas AKAP-*IS* had some affinity for RIα (lane 2), RIα binding was abolished for SuperAKAP-*IS* (lane 4). AKAP-*IS* and SuperAKAP-*IS* appeared to bind with similar strength to RIIα in the R overlay (lane 2 and 4, respectively).

Next, the characteristics of SuperAKAP-*IS* as a competitor were analyzed by adding peptide (1 μM) to RIIα-^{32}P in solution before an overlay experiment was performed (Figure 7B). SuperAKAP-*IS* in solution competed most of the RIIα-^{32}P binding to SuperAKAP-*IS* synthesized on membrane in concentrations of 0.5 (data not shown) to 1 μM (Figure 7B). SuperAKAP-*IS* synthesized on membrane also bound human RIIα with a similar affinity as for mouse RIIα, indicating that this peptide should be able to compete and displace RIIα-AKAP interactions in situ both in human and rodent cells (data not shown). In contrast to AKAP-*IS*, SuperAKAP-*IS* revealed no binding to human RIα (data not shown).

Having established that SuperAKAP-*IS* binds specifically to RIIα and not to RIα in vitro, it was important to test whether this peptide could selectively disrupt type II PKA anchoring inside cells. A cell-permeable SuperAKAP-*IS* derivative was generated by coupling 11 arginine residues to the N terminus of the peptide (Arg_{11}-SuperAKAP-*IS*). Previous studies have shown that the addition of a polybasic sequence renders the peptide derivatives cell soluble. The PKA anchoring disruptor properties of Arg_{11}-SuperAKAP-*IS* were compared to arginine-coupled derivatives of AKAP-*IS*, Ht31, and a recently described RI-selective anchoring disruptor peptide called RIAD (Carlson et al., 2006) (Figure 7C). Application of Arg_{11}-SuperAKAP-*IS* displaced PKA-RIIα from the cell membrane of human T cells at concentrations of 25–50 μM as demonstrated by immunofluorescence (Figure 7C, top two rows) when compared to untreated cells (Figure 7C, left column). In contrast, no displacement of PKA-RIα was observed in cells treated with Arg_{11}-SuperAKAP-*IS* (Figure 7C, bottom row). Conversely, the RI-selective competitor peptide RIAD displaced RIα, but not RIIα as assessed by the immunofluoresence assay. As anticipated, AKAP-*IS* and Ht31

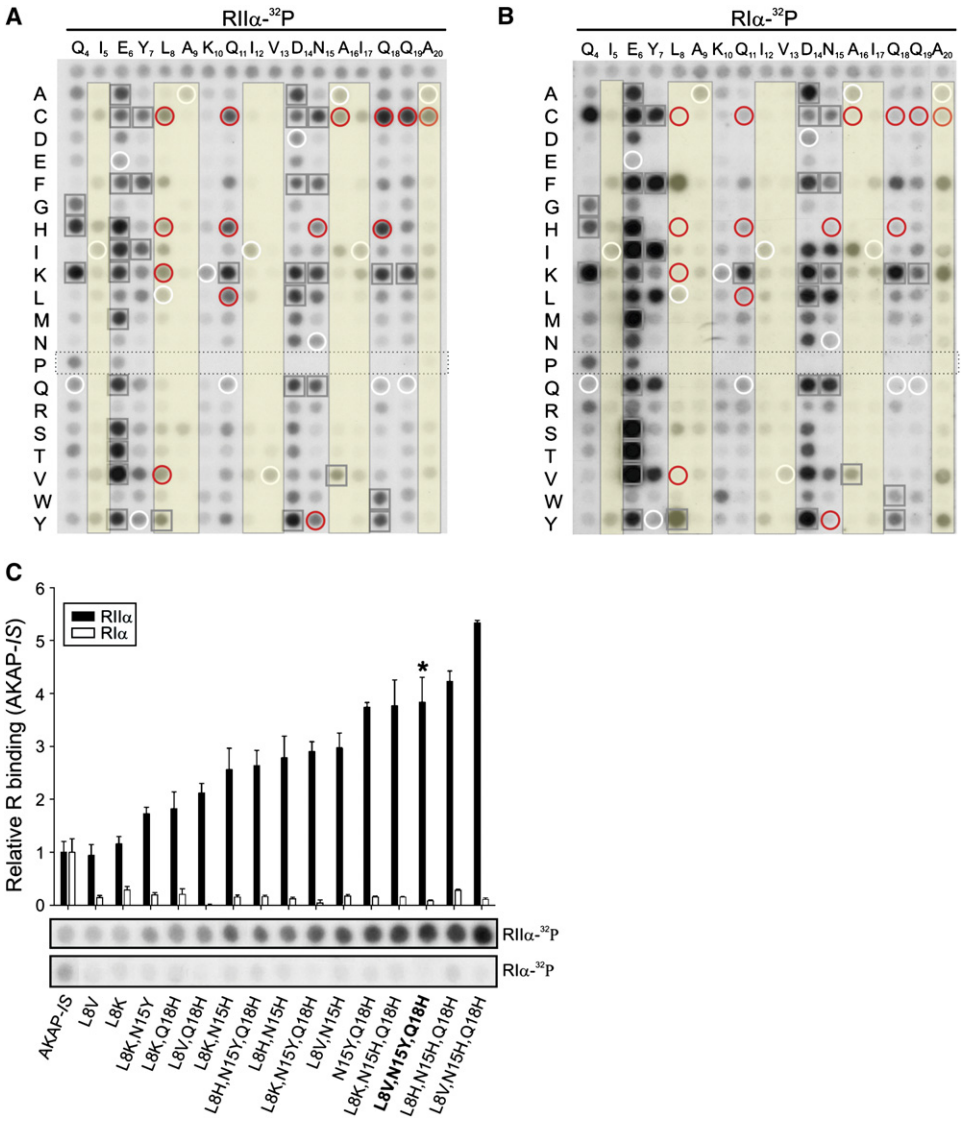

Figure 6. Optimization of AKAP-*IS* Sequence to Yield an RII-Specific Peptide

Two-dimensional arrays of 340 AKAP-*IS* peptide derivatives where each residue in AKAP-*IS* (above each array) was replaced with all 20 amino acids (indicated to the left of each array) are shown. The first row in each array corresponds to the native peptide (AKAP-*IS*). R subunit binding was analyzed by either (A) RIIα-^{32}P or (B) RIα-^{32}P overlay and signal detected by autoradiography. Peptide derivatives with higher (or unchanged) RIIα affinity and lower RIα affinity (red circles) or higher affinity for both RIα and RIIα (black squares) are indicated. Internal control peptides of the starting sequence (white circles), positions of hydrophobic amino acids in AKAP-*IS* (yellow columns) and proline substitution (dotted rectangle) are indicated. (C) The RIIα-^{32}P (top) and RIα-^{32}P (bottom) binding of the original AKAP-*IS* sequence and 15 peptide derivatives (single, double, and triple substitutions) with lower affinity for RIα and higher affinity for RIIα are shown. The relative RIα and RIIα binding affinities were measured by densitometry analysis of the autoradiographs (means ± STD from n = 3). Binding of RIIα and RIα to AKAP-*IS* was arbitrarily set to one for this comparison. Note that affinity of AKAP-*IS* to RIIα and RIα differs (Alto et al., 2003). Star denotes peptide selected for further characterization (named SuperAKAP-*IS*).

disrupted RI and RII anchoring in these cells (Figure 7C, middle panels).

Although our immunofluorescence study did not appear to detect any significant differences in the potency of SuperAKAP-*IS* and AKAP-*IS* as competitors of RII anchoring, we were able to conclude that Arg_{11}-SuperAKAP-*IS* is a potent and selective RII anchoring disruptor peptide. This latter observation is supported by evidence that both peptides display subnanomolar affinities for RIIα when assessed by in-solution fluorescence polarization (data not shown). Nonetheless, SuperAKAP-*IS* is the most selective RII-directed anchoring disruptor reagent developed to date and can be used as a tool to delineate cellular effects mediated by anchored pools of type II PKA holoenzyme.

We next attempted to uncouple anchored signaling events that are attributed to the PKA type II holoenzyme. A physiologically relevant model is the time-dependent downregulation (run down) of α-amino-3-hydroxy-5-methyl-4-isoxazolepropionic acid (AMPA)-responsive currents in hippocampal neurons after addition of glutamate. This requires an anchored pool of type II PKA as demonstrated by anchoring disruption using the Ht31 anchoring disruption peptide (Rosenmund et al., 1994).

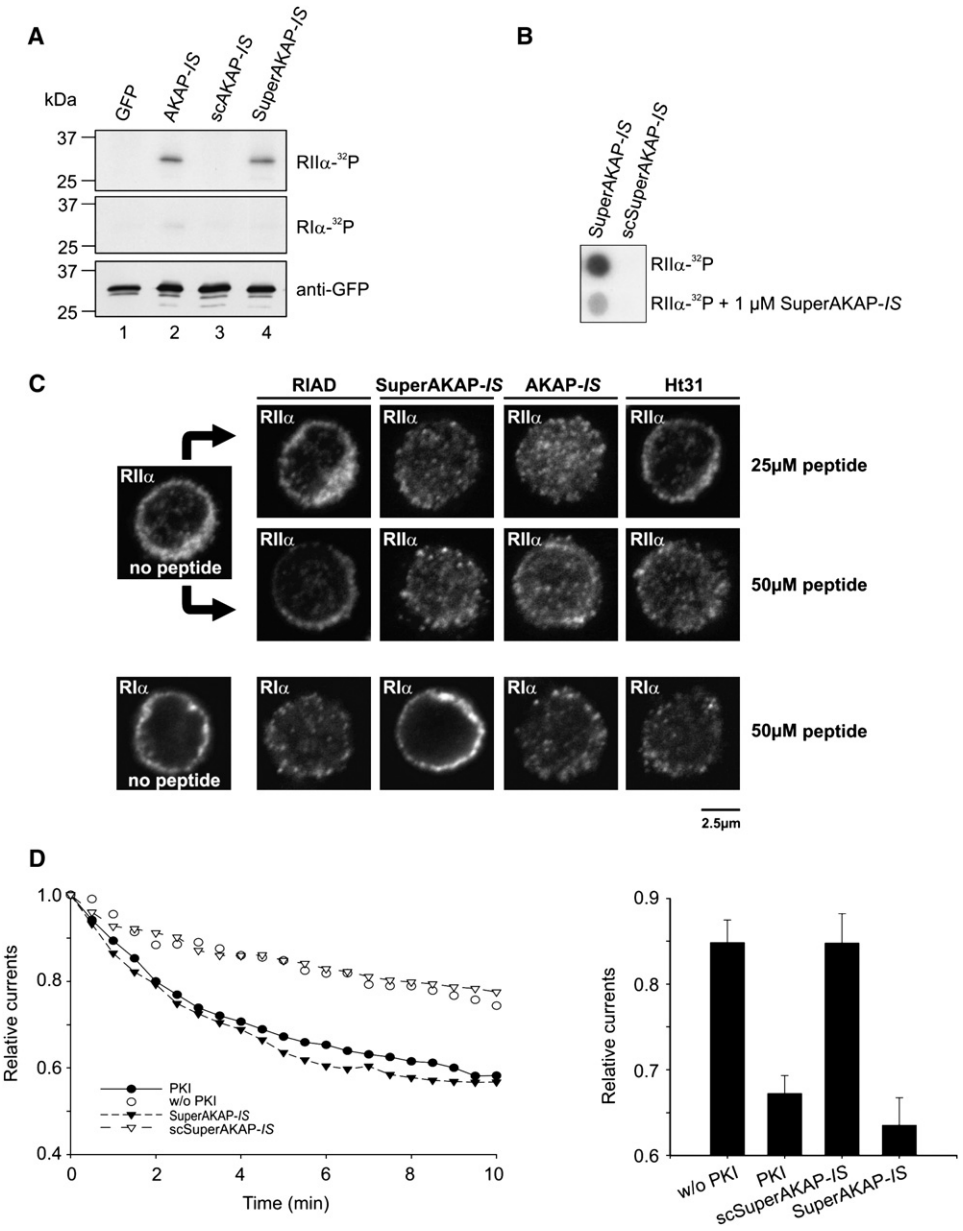

Figure 7. Functional Characterization of SuperAKAP-*IS*

(A) Lysates from HEK293 cells transfected with GFP, GFP-AKAP-*IS*, GFP-scAKAP-*IS*, and GFP-SuperAKAP-*IS* were analyzed for R binding by RIIα-^{32}P or RIα-^{32}P overlay. Immunoblotting using GFP antibody was used as loading control (bottom).

(B) SuperAKAP-*IS* and its scrambled peptide were synthesized on membranes. RII binding was detected by RIIα-^{32}P overlay in absence (top row) or presence of 1 μM SuperAKAP-*IS* peptide in the solution.

(C) Subcellular localization of PKA-RIIα (top two rows) and PKA-RIα (bottom row) in human peripheral blood T cells that received no peptide (left) or were treated (right) with 25 μM (top row) or 50 μM (two bottom rows) Arg_{11}-coupled competitor peptides RIAD, SuperAKAP-*IS*, AKAP-*IS*, or Ht31 and analyzed by immunofluorescence.

(D) The effect of SuperAKAP-*IS* on time-dependent run down of AMPA-responsive currents in hippocampal neurons was analyzed by using whole-cell patch-clamp recording techniques (left). PKI (PKA inhibitor) was used as a positive control, and the scrambled control peptide scSuperAKAP-*IS* was used as negative control. Averaged peak currents from 0 to 10 min are shown. Graphical representation of the peak current amplitudes upon glutamate stimulation 5 min after delivery of the peptides (indicated below each column, right). Each bar is normalized to the peak amplitude found at time 0. PKI was used at 10 μM, and other peptides were used at a concentration of 1 μM (means ± SEM from n = 4–11).

Whole-cell patch-clamp techniques provided a sensitive means to record the current upon delivery of the different bioactive peptides through the patch pipette. Perfusion of SuperAKAP-*IS* (1 μM) caused rapid reduction in the AMPA-responsive currents to a similar extent as PKI (PKA inhibitor) included as control, indicating the ability of SuperAKAP-*IS* to interfere with PKA type II-mediated regulation of ion-channel conductivity (Figure 7D). Additional control experiments demonstrated that scrambled peptide (scSuperAKAP-*IS*, negative control) was unable to affect AMPA-responsive currents (Figure 6D). Thus, SuperAKAP-*IS* appears to be able to

specifically block cellular functions mediated by the type II PKA holoenzyme.

Discussion

The RIIα-AKAP-*IS* complex structure described here provides a molecular framework for understanding the specificity determinants for RII, RI, and dual-selective AKAPs. This study also provides a compelling rationalization for the results of peptide array AKAP-RII and RI interaction screens. All AKAPs feature nonpolar residues at positions 5, 9, 12, 13, 16, 17, and 20 (Figure 2A), which in our structure form a hydrophobic ridge for docking onto the nonpolar RII-AKAP binding interface (Figure 3A). Strikingly, RII-peptide array screening data indicated that high-affinity AKAP-RII interactions are not compatible with bulky residues at these positions (this study; Burns-Hamuro et al., 2003; Alto et al., 2003), consistent with the intimate contacts between AKAP-*IS* and RIIα. Interestingly, the RII-peptide array screen revealed that the affinity of RII-AKAP interactions was particularly sensitive to substitutions of AKAP residues at positions 9, 13, and 16 (this study and Alto et al. [2003]). At positions 9 and 16, an Ala is preferred and only the small Gly, Thr, and Ser residues are tolerated. A Val is strongly preferred at position 13, with Ala, Ile, Thr, and Cys being weakly tolerated (Alto et al., 2003) (Figure 6A). In the structure, Ala9, Val13, and Ala16 are deeply buried at the RII-AKAP interface, suggesting that residues larger than Ala or Val at these positions could not be readily accommodated. Ala9, Val13, and Ala16 are highly conserved in RII-specific AKAPs (Figure 2A).

Ile17 is more solvent exposed, explaining the greater variability of residues tolerated at this position. Burns-Hamuro and colleagues discovered that while a Trp at position 17 was compatible with RI binding, RII binding was eliminated (Burns-Hamuro et al., 2003). Ile17 engages a hydrophobic pocket defined by $Ile5^{R}$ and $Leu9^{R}$ in RIIα (Figure 4B). The equivalent residues in RIα are Gln and Ile, suggesting that in RI there exists a larger more-hydrophilic pocket capable of accommodating the large and partially polar Trp side chain.

Our structure also provides insights into how the three mutants of AKAP-*IS* generate the more affine RII binding SuperAKAP-*IS* while abolishing its affinity for RI. The Leu8Val mutation led to a large drop in binding affinity for RIα but had little effect on RIIα binding. This finding suggested that in RIIα the loop containing $Ile3^{R'}$ and $Ile5^{R'}$ can reorganize to accommodate Val8. Despite low sequence identity between the RII and RI D/D domains, the N-terminal loop of αA′ is positioned similarly to the helical isoform-specific docking region proposed in the RI NMR structure (Banky et al., 2003). Peptide screening showed that RI binding was enhanced by larger nonpolar residues such as Phe and Tyr (Figure 5B and Burns-Hamuro et al. [2003]). This suggests that a substitution of Val for Leu at position 8 results in the loss of high-affinity nonpolar packing interactions between AKAP and RI.

The Asn15Tyr and Gln18His mutations led to an increase in affinity for RIIα, despite the crystal structure indicating that the Asn15Tyr substitution would break an intrahelical H bond. This may be compensated for by the formation of a direct H bond from Tyr15 to $Thr10^{R'}$ in RIIα or by the formation of an intrahelical stacking interaction between Tyr15 and His18. His18 is suitably placed to cap the helix at the C terminus; however, the crystal structure is not informative in this respect, as an additional lysine has been included at the C terminus to improve solubility of the peptide for crystallization.

The AKAP-*IS* interactions to $Thr10^{R}$ and $Gln14^{R}$ at the corners of the RIIα interface add an intriguing extra level of subtlety to the RII interface (Figure 2D). For RI, the equivalent pairs are Gly and Lys, respectively. Alignment of dual, RII- and RI-specific AKAP peptides (Figure 2A) reveals striking differences in AKAP positions 15 and 19 that contact these residues. Acidic residues predominate at position 19 of dual and RI-specific AKAPs (Figure 2A), and these in principle could salt bridge to Lys14R of RI (equivalent to $Gln14^{R}$ of RII). In RII-specific AKAPs, Asn15 and Gln19 are favored, which we observe to H bond to $Thr10^{R'}$ and $Gln14^{R'}$ in RII (Figure 2D). This suggests a mechanism by which polar interactions outside of the hydrophobic core distinguish between the RI and RII isoforms.

In general, AKAP proteins bind more tightly to RII than RI. Although RI-selective peptides have been engineered (Burns-Hamuro et al., 2003; Carlson et al., 2006), the only naturally occurring RI-selective AKAP that has been conclusively shown to have a poor K_d for RII is AKAPce (Angelo and Rubin, 1998). However, this may be the exception rather than the rule, as there is only one R subunit isoform in *C. elegans*, which is marginally more similar to RI than RII. Both the $Ile3^{R'}$/$Ile5^{R'}$ loop and $Thr10^{R}$-$Gln14^{R}$ pairs in RIIα are compatible with a range of substitutions in the appropriate positions in AKAP (Figure 2C), whereas peptide screening indicates that RI is less accommodating in the equivalent positions (Burns-Hamuro et al., 2003). This correlates with the ability of RII to bind to a broad range of AKAPs with high affinity.

RI and RII differ physiologically in both their localization (Skalhegg and Tasken, 2000) and cAMP responsiveness (Feliciello et al., 2001). In tandem with RI-specific AKAP peptides such as RIAD (Carlson et al., 2006), SuperAKAP-*IS* will, with its demonstrated specificity for RII, be a useful in vivo reagent for assessing the contribution of anchoring of the different R subunit isoforms in various cellular processes. Further structural studies of D/D complexes will clarify the mechanisms that determine AKAP affinity and specificity. These may include sp17, a non-PKA D/D domain shown to bind AKAPs (Frayne and Hall, 2002), and Rfc40, reported to bind the D/D domain of RI (Gupte et al., 2005).

Experimental Procedures

Protein Expression and Purification

Murine RIIα (1^{R}-43^{R}) was cloned into pET30 incorporating a C-terminal $RGLEH_6$ sequence. The protein was purified by Ni-NTA and Superdex 75 chromatography. Human RIIα (1^{R}-45^{R}) was cloned into pGEX6P3 and expressed as GST-fusion protein (Amersham Biosciences). The protein was purified by using glutathione Sepharose (Amersham Biosciences), and bound protein was cleaved from the beads overnight with PreScission (Amersham Biosciences) and finally purified by size-exclusion chromatography on Superdex 75 in 15 mM Tris-HCl (pH 7.5), 200 mM NaCl, 0.5 mM EDTA, and 2 mM DTT. For noncrystallographic work, bovine, murine, or human R protein was expressed in *E. coli* BL21 by IPTG induction and purified with cAMP beads.

Protein Crystallization

Apo RIIα was crystallized by vapor diffusion with 8%–10% PEG 400, 0.2–0.4 M sodium phosphate, and sodium citrate (pH 5.8), and crystals were flash-frozen with cryo-protection buffer consisting of 20% mother liquor and 80% saturated lithium acetate. Crystals of the RIIα (1^R-45^R)-AKAP-*IS* (sequence: QIEYLAKQIVDNAIQQAK) complex were initially obtained by hanging drop vapor diffusion by selecting for crystals that only appeared when the AKAP-*IS* peptide was present. The best diffracting crystals were grown at 4°C in 1 M trisodium citrate, 0.1 M Tris-HCl (pH 7.5), with RII:AKAP in a 4:3 molar ratio and RIIα (1^R-45^R) at 15 mg/ml. For cryoprotection, crystals were immersed for 2 min in 1 M trisodium citrate, 150 mM NaCl, 0.1 M Tris-HCl (pH 7.5), and 25% glycerol.

Data Collection and Structure Determination

Apo RIIα (1^R-43^R)

To determine the crystal structure, we substituted Met individually for each of the three Leu residues (Leu 9^R, 12^R, and 28^R). The structure was solved with MAD data by means of SHELXS and SOLVE software and refined by using CNS. These refined coordinates were used to determine the native wild-type RII D/D crystal structure and refined to 2.2 Å with REFMAC (Table 1). NCS restraints were applied during initial refinement stages but removed during the final stages of refinement. The regions of RII D/D that are visible in the electron density map are listed in Table S1.

RIIα (1^R-45^R)-AKAP-IS

Data were processed by using MOSFLM and scaled and merged in SCALA (CCP4, 1994). The structure was solved by molecular replacement with PHASER (McCoy et al., 2005) using apo RII as the search model. The AKAP-*IS* peptide and additional residues were manually built by using COOT, and the complex structure was refined in REFMAC5 with anisotropic B factors (Table 1). The model includes two DTT molecules, assigned by apparent electron density. All molecular representations in figures were created by using the PyMOL Molecular Graphics System (DeLano Scientific, http://www.pymol.org).

Autospot Peptide Array

Peptide arrays were synthesized on cellulose paper by using an Autospot Robot ASP222 or a Multipep automated peptide synthesizer (INTAVIS Bioanalytical Instruments AG) as described (Frank, 2002).

Densitometric Analysis

The densitometric analysis was performed with Scion Image (Scion Coorperation, http://www.scioncorp.com) or Quantity One version 4.5.0 (BioRad).

R Overlay

R overlays were conducted as described, using ^{32}P-labeled recombinant murine or human RIIα (Hausken et al., 1998) or recombinant bovine or human RIα (A98S) (Carlson et al., 2006). Briefly, the membrane was blocked in blotto (5% [w/v] nonfat dry milk plus 0.1% bovine serum albumin in Tris-buffered saline [TBS]). Purified recombinant R (4 μg) was radiolabeled with purified catalytic subunit (C) of PKA (0.02 μg/μl) and [γ-^{32}P] ATP (1.4 μCi μl^{-1}) in 50 mM MOPS, 50 mM NaCl, 2 mM $MgCl_2$, and 1 mM DTT (pH 6.8) and separated from free ^{32}P-ATP by gel filtration (G-50 Sepharose). The membrane was washed in TBS with 0.1% Tween-20 (TBST) and signal detected by autoradiography. Because affinities of AKAP-*IS* and derivates were high for RII and low for RI, exposure times for peptide arrays overlayed with RII were 5–10 min, whereas exposure times for arrays overlaid with RI were 3–12 hr.

Cell Cultures and Transient Transfections

HEK293 cells were maintained in DMEM supplemented with 100 μg/ml streptomycin, 100 U/ml penicillin, and 10% (v/v) fetal calf serum in a humidified atmosphere of 5% CO_2 and split by trypsination at less than 80% confluence. HEK293 cells at 50%–80% confluency were transfected with 10 μg of plasmid DNA (GFP, GFP-SuperAKAP-*IS*, GFP-AKAP-*IS*, and GFP-scrambled AKAP-*IS*) per 56.7 cm^2 culture dishes by using the $CaCl_2$ method. Cells were lysed after 30 hr in lysis buffer (20 mM HEPES [pH 7.5], 150 mM NaCl, 1 mM EDTA, and 1% Triton X-100) with protease inhibitors (Complete Mini, EDTA-free tablets, Roche).

Immunoblot Analysis

Cell lysates were analyzed on 15% PAGE and blotted onto PVDF membranes. The filters were blocked in 5% nonfat dry milk in TBST for 30 min at RT, incubated 1 hr at RT or overnight at 4°C with anti-GFP monoclonal antibody (Clontech) at a 1 μg ml^{-1} dilution for immunoblotting, washed four times for 5 min in TBST, and incubated with HRP-conjugated anti-mouse as secondary antibodies at a 1:5000 dilution (Jackson Immunoresearch). Blots were developed by using Supersignal West Pico substrate (Pierce).

Peptide Synthesis

SuperAKAP-*IS*, scrambled SuperAKAP-*IS* (scSuperAKAP-*IS: QDVE IHVKAAYYQQIAI*), Arg_{11}-AKAP-*IS*, Arg_{11}-SuperAKAP-*IS*, Arg_{11}-Ht31 (Arg_{11}-LIEEAASRIVDAVIEQV), and RIAD-Arg_{11} (LEQYANQLAD QIIKEATE-Arg_{11}) were synthesized and purified to >80% purity (SynPep, or in house at the Biotechnology Centre). The peptide concentrations used were exactly determined by amino acid analysis using Applied Biosystems Analyzer 421. AKAP-*IS* was synthesized at high purity (>90%) for crystallization (Jacky Metcalfe, Institute of Cancer Research, Sutton).

Immunofluorescence

Immunofluorescence was performed on human peripheral blood T cells purified as described (Aandahl et al., 1998). Arginine-coupled peptides were added to the cell culture and incubated for 1 hr. Cells were attached to polylysin-coated coverslips, washed in PBS, fixed with 3% paraformaldehyde, and permeabilized using 0.1% Triton X-100. Proteins were blocked in 2% BSA/PBST prior to antibody labeling. Mouse primary antibody against RIα (clone 4D7 [Skalhegg et al., 1994; Tasken et al., 1993]), RIIα (BD Transduction Laboratories), and Alexa 488 anti-mouse IgG secondary antibody (Molecular Probes, Invitrogen) were used at 1:200 and 1:500 dilution, respectively, in BSA/PBST and incubated for 30 min. Cells were examined using a Zeiss LSM 510 META confocal fluorescence microscope.

Electrophysiology

Whole-cell recordings were made with an Axopatch200B amplifier (Axon Instruments). Patch pipettes (2-4 MΩ) contained (in mM) 140 cesium methanesulfonate, 5 adenosine triphosphate, 5 $MgCl_2$, 0.2 $CaCl_2$, 1 BAPTA (1,2-bis[2-aminophenoxy]ethane-*N,N,N',N'*-tetraacetate), and 10 HEPES (pH 7.4). Extracellular solution contained (in mM) 150 NaCl, 5 KCl, 1.8 $CaCl_2$, 10 glucose, 0.1 cyclothiazide, and 10 HEPES (pH 7.4). Solution exchanges were accomplished through a two-barrel pipe controlled by a solution stimulus delivery device, SF-77B (Warner Instruments,). The GluR1 (AMPA channel subunit) receptor currents were evoked by a 500 ms application of 1 mM glutamate at 30 s intervals. Data were acquired and analyzed by using PCLAMP software (Axon Instruments). Currents were digitized at 5 kHz and filtered at 1 kHz.

Supplemental Data

Supplemental Data include one table and can be found with this article online at http://www.molecule.org/cgi/content/full/24/3/383/DC1/.

Acknowledgments

This work has been supported by The Medical Research Council, Cancer Research-UK, The Norwegian Cancer Society, and Oddrun Mjålands Stiftelse and by grants from the National Institutes of Health (grant number DK54441), The National Programme for Research in Functional Genomics in Norway (FUGE), The Research Council of Norway, and the European Union (RTD grant number QLK3-CT-2002-02149). We thank Torunn Berge for help with the immunofluorescence experiment, Robert Mouton (Scott lab) for technical assistance, and Maruf Ali (ICR) for help with data collection.

Received: April 11, 2006
Revised: July 28, 2006
Accepted: September 14, 2006
Published: November 2, 2006

References

Aandahl, E.M., Aukrust, P., Skalhegg, B.S., Muller, F., Froland, S.S., Hansson, V., and Tasken, K. (1998). Protein kinase A type I antagonist restores immune responses of T cells from HIV-infected patients. FASEB J. *12*, 855–862.

Alto, N., Carlisle Michel, J.J., Dodge, K.L., Langeberg, L.K., and Scott, J.D. (2002). Intracellular targeting of protein kinases and phosphatases. Diabetes *51* (*Suppl 3*), S385–S388.

Alto, N.M., Soderling, S.H., Hoshi, N., Langeberg, L.K., Fayos, R., Jennings, P.A., and Scott, J.D. (2003). Bioinformatic design of A-kinase anchoring protein-in silico: a potent and selective peptide antagonist of type II protein kinase A anchoring. Proc. Natl. Acad. Sci. USA *100*, 4445–4450.

Angelo, R., and Rubin, C.S. (1998). Molecular characterization of an anchor protein (AKAPCE) that binds the RI subunit (RCE) of type I protein kinase A from Caenorhabditis elegans. J. Biol. Chem. *273*, 14633–14643.

Banky, P., Roy, M., Newlon, M.G., Morikis, D., Haste, N.M., Taylor, S.S., and Jennings, P.A. (2003). Related protein-protein interaction modules present drastically different surface topographies despite a conserved helical platform. J. Mol. Biol. *330*, 1117–1129.

Burns, L.L., Canaves, J.M., Pennypacker, J.K., Blumenthal, D.K., and Taylor, S.S. (2003). Isoform specific differences in binding of a dual-specificity A-kinase anchoring protein to type I and type II regulatory subunits of PKA. Biochemistry *42*, 5754–5763.

Burns-Hamuro, L.L., Ma, Y., Kammerer, S., Reineke, U., Self, C., Cook, C., Olson, G.L., Cantor, C.R., Braun, A., and Taylor, S.S. (2003). Designing isoform-specific peptide disruptors of protein kinase A localization. Proc. Natl. Acad. Sci. USA *100*, 4072–4077.

Carlson, C.R., Lygren, B., Berge, T., Hoshi, N., Wong, W., Tasken, K., and Scott, J.D. (2006). Delineation of type I protein kinase A-selective signaling events using an RI anchoring disruptor. J. Biol. Chem. *281*, 21535–21545.

Carnegie, G.K., Smith, F.D., McConnachie, G., Langeberg, L.K., and Scott, J.D. (2004). AKAP-Lbc nucleates a protein kinase D activation scaffold. Mol. Cell *15*, 889–899.

Carr, D.W., Stofko-Hahn, R.E., Fraser, I.D., Bishop, S.M., Acott, T.S., Brennan, R.G., and Scott, J.D. (1991). Interaction of the regulatory subunit (RII) of cAMP-dependent protein kinase with RII-anchoring proteins occurs through an amphipathic helix binding motif. J. Biol. Chem. *266*, 14188–14192.

CCP4 (Collaborative Computation Project, Number 4) (1994). The CCP4 suite: programs for protein crystallography. Acta. Crystallogr. D Biol. Crystallogr. *50*, 760–763.

Dodge-Kafka, K.L., Soughayer, J., Pare, G.C., Carlisle Michel, J.J., Langeberg, L.K., Kapiloff, M.S., and Scott, J.D. (2005). The protein kinase A anchoring protein mAKAP coordinates two integrated cAMP effector pathways. Nature *437*, 574–578.

Fayos, R., Melacini, G., Newlon, M.G., Burns, L., Scott, J.D., and Jennings, P.A. (2003). Induction of flexibility through protein-protein interactions. J. Biol. Chem. *278*, 18581–18587.

Feliciello, A., Gottesman, M.E., and Avvedimento, E.V. (2001). The biological functions of A-kinase anchor proteins. J. Mol. Biol. *308*, 99–114.

Fink, M.A., Zakhary, D.R., Mackey, J.A., Desnoyer, R.W., Apperson-Hansen, C., Damron, D.S., and Bond, M. (2001). AKAP-mediated targeting of protein kinase a regulates contractility in cardiac myocytes. Circ. Res. *88*, 291–297.

Frank, R. (2002). The SPOT-synthesis technique. Synthetic peptide arrays on membrane supports–principles and applications. J. Immunol. Methods *267*, 13–26.

Frayne, J., and Hall, L. (2002). A re-evaluation of sperm protein 17 (Sp17) indicates a regulatory role in an A-kinase anchoring protein complex, rather than a unique role in sperm-zona pellucida binding. Reproduction *124*, 767–774.

Gupte, R.S., Weng, Y., Liu, L., and Lee, M.Y. (2005). The second subunit of the replication factor C complex (RFC40) and the regulatory subunit (RIalpha) of protein kinase A form a protein complex promoting cell survival. Cell Cycle *4*, 323–329.

Hausken, Z.E., Coghlan, V.M., Hastings, C.A., Reimann, E.M., and Scott, J.D. (1994). Type II regulatory subunit (RII) of the cAMP-dependent protein kinase interaction with A-kinase anchor proteins requires isoleucines 3 and 5. J. Biol. Chem. *269*, 24245–24251.

Hausken, Z.E., Dell'Acqua, M.L., Coghlan, V.M., and Scott, J.D. (1996). Mutational analysis of the A-kinase anchoring protein (AKAP)-binding site on RII. Classification Of side chain determinants for anchoring and isoform selective association with AKAPs. J. Biol. Chem. *271*, 29016–29022.

Hausken, Z.E., Coghlan, V.M., and Scott, J.D. (1998). Overlay, ligand blotting, and band-shift techniques to study kinase anchoring. Methods Mol. Biol. *88*, 47–64.

Herberg, F.W., Maleszka, A., Eide, T., Vossebein, L., and Tasken, K. (2000). Analysis of A-kinase anchoring protein (AKAP) interaction with protein kinase A (PKA) regulatory subunits: PKA isoform specificity in AKAP binding. J. Mol. Biol. *298*, 329–339.

Huang, L.J., Durick, K., Weiner, J.A., Chun, J., and Taylor, S.S. (1997). D-AKAP2, a novel protein kinase A anchoring protein with a putative RGS domain. Proc. Natl. Acad. Sci. USA *94*, 11184–11189.

Johnson, B.D., Scheuer, T., and Catterall, W.A. (1994). Voltage-dependent potentiation of L-type Ca2+ channels in skeletal muscle cells requires anchored cAMP-dependent protein kinase. Proc. Natl. Acad. Sci. USA *91*, 11492–11496.

Kammerer, S., Burns-Hamuro, L.L., Ma, Y., Hamon, S.C., Canaves, J.M., Shi, M.M., Nelson, M.R., Sing, C.F., Cantor, C.R., Taylor, S.S., and Braun, A. (2003). Amino acid variant in the kinase binding domain of dual-specific A kinase-anchoring protein 2: a disease susceptibility polymorphism. Proc. Natl. Acad. Sci. USA *100*, 4066–4071.

Kinderman, F.S., Kim, C., von Daake, S., Ma, Y., Pham, B.Q., Spraggon, G., Xuong, N.-H., Jennings, P.A., and Taylor, S.S. (2006). A dynamic mechanism for AKAP binding to RII isoforms of cAMP-dependent protein kinase. Mol. Cell *24*, this issue, 397–408.

Klauck, T.M., Faux, M.C., Labudda, K., Langeberg, L.K., Jaken, S., and Scott, J.D. (1996). Coordination of three signaling enzymes by AKAP79, a mammalian scaffold protein. Science *271*, 1589–1592.

Li, H., Degenhardt, B., Tobin, D., Yao, Z.X., Tasken, K., and Papadopoulos, V. (2001). Identification, localization, and function in steroidogenesis of PAP7: a peripheral-type benzodiazepine receptor- and PKA (RIalpha)-associated protein. Mol. Endocrinol. *15*, 2211–2228.

Lohmann, S.M., DeCamilli, P., Einig, I., and Walter, U. (1984). High-affinity binding of the regulatory subunit (RII) of cAMP-dependent protein kinase to microtubule-associated and other cellular proteins. Proc. Natl. Acad. Sci. USA *81*, 6723–6727.

McCoy, A.J., Grosse-Kunstleve, R.W., Storoni, L.C., and Read, R.J. (2005). Likelihood-enhanced fast translation functions. Acta Crystallogr. D Biol. Crystallogr. *61*, 458–464.

Miki, K., and Eddy, E.M. (1999). Single amino acids determine specificity of binding of protein kinase A regulatory subunits by protein kinase A anchoring proteins. J. Biol. Chem. *274*, 29057–29062.

Moita, M.A., Lamprecht, R., Nader, K., and LeDoux, J.E. (2002). A-kinase anchoring proteins in amygdala are involved in auditory fear memory. Nat. Neurosci. *5*, 837–838.

Newlon, M.G., Roy, M., Morikis, D., Carr, D.W., Westphal, R., Scott, J.D., and Jennings, P.A. (2001). A novel mechanism of PKA anchoring revealed by solution structures of anchoring complexes. EMBO J. *20*, 1651–1662.

Pawson, T., and Scott, J.D. (1997). Signaling through scaffold, anchoring, and adaptor proteins. Science *278*, 2075–2080.

Ranganathan, G., Pokrovskaya, I., Ranganathan, S., and Kern, P.A. (2005). Role of A kinase anchor proteins in the tissue-specific regulation of lipoprotein lipase. Mol. Endocrinol. *19*, 2527–2534.

Rosenmund, C., Carr, D.W., Bergeson, S.E., Nilaver, G., Scott, J.D., and Westbrook, G.L. (1994). Anchoring of protein kinase A is required for modulation of AMPA/kainate receptors on hippocampal neurons. Nature *368*, 853–856.

Shabb, J.B. (2001). Physiological substrates of cAMP-dependent protein kinase. Chem. Rev. *101*, 2381–2411.

Skalhegg, B.S., and Tasken, K. (2000). Specificity in the cAMP/PKA signaling pathway. Differential expression,regulation, and subcellular localization of subunits of PKA. Front. Biosci. *5*, D678–D693.

Skalhegg, B.S., Tasken, K., Hansson, V., Huitfeldt, H.S., Jahnsen, T., and Lea, T. (1994). Location of cAMP-dependent protein kinase type I with the TCR-CD3 complex. Science *263*, 84–87.

Smith, F.D., Langeberg, L.K., and Scott, J.D. (2006). The where's and when's of kinase anchoring. Trends Biochem. Sci. *31*, 316–323.

Tasken, K., Skalhegg, B.S., Solberg, R., Andersson, K.B., Taylor, S.S., Lea, T., Blomhoff, H.K., Jahnsen, T., and Hansson, V. (1993). Novel isozymes of cAMP-dependent protein kinase exist in human cells due to formation of RI alpha-RI beta heterodimeric complexes. J. Biol. Chem. *268*, 21276–21283.

Vallee, R.B., DiBartolomeis, M.J., and Theurkauf, W.E. (1981). A protein kinase bound to the projection portion of MAP 2 (microtubule-associated protein 2). J. Cell Biol. *90*, 568–576.

Westphal, R.S., Tavalin, S.J., Lin, J.W., Alto, N.M., Fraser, I.D., Langeberg, L.K., Sheng, M., and Scott, J.D. (1999). Regulation of NMDA receptors by an associated phosphatase-kinase signaling complex. Science *285*, 93–96.

Wong, W., and Scott, J.D. (2004). AKAP signalling complexes: focal points in space and time. Nat. Rev. Mol. Cell Biol. *5*, 959–970.

Zhang, J., Hupfeld, C.J., Taylor, S.S., Olefsky, J.M., and Tsien, R.Y. (2005). Insulin disrupts beta-adrenergic signalling to protein kinase A in adipocytes. Nature *437*, 569–573.

Accession Numbers

Coordinates and structure factors have been deposited with the PDB under accession codes 2izy, r2izysf (apo) and 2izx, r2izxsf (complex).